


RESEARCH ARTICLE

Adaptive robust control for Pendubot with matched–mismatched uncertainty via constraint-following

Cui Wei^{1,*} , Ye-Hwa Chen², Tianyou Chai³ and Jun Fu³

¹Institute of Intelligent Manufacturing, Nanjing Tech University, Nanjing 210009, China, ²George W. Woodruff School of Mechanical Engineering, Georgia Institute of Technology, Atlanta, GA 30332, USA, and ³State Key Laboratory of Synthetical Automation for Process Industries, Northeastern University, Shenyang 110819, China

*Corresponding author. E-mail: cwei@njtech.edu.cn

Received: 22 June 2022; **Revised:** 11 November 2022; **Accepted:** 16 December 2022; **First published online:** 17 January 2023

Keywords: constraint-following, underactuated, Pendubot, matched–mismatched uncertainty, adaptive robust control

Abstract

The study presents an adaptive robust control method for the Pendubot subjects to matched and mismatched uncertainty. First, the control task is formatted as a reduced-dimension equality constraint of the system states. To handle the matched and mismatched uncertainties, an orthogonal decomposition method is employed to make the mismatched part disappear after decomposition. Based on the above, an adaptive robust control law based on constraint-following is devised. By the Lyapunov approach, it is rigorously proven that the proposed approach ensures the uniform boundedness and uniform ultimate boundedness of the closed-loop control system and thus renders approximate constraint-following, regardless of uncertainty. Simulation and experimental results are provided and discussed, demonstrating the good performance of the proposed approach.

1. Introduction

Underactuated mechanical systems have fewer independent actuators than the degrees of freedom [1, 2]. Due to the reduction of actuators, these systems have some important merits which include lighter weight, lower cost, and less energy consumption and thus have been widely applied in industries [3], such as cranes [4], robots [5, 6], hovercrafts [7], surface/underwater vehicles [8, 9], and spacecrafts [10]. The Pendubot system is a classical two-link underactuated robot with only one actuator [11]. Due to the strong nonlinear coupling relationship between the two links, even though the actuated link is stabilized at the desired position, it is hard to guarantee the stability of the unactuated one. Consequently, the control problem of the Pendubot has received growing attention in recent years.

In refs. [11], [12], and [13], feedback control, energy-based control, and impulse momentum methods are proposed to stabilize the Pendubot. Nevertheless, none of them takes account of system uncertainties. Uncertainty, such as dynamic friction, external disturbances, and initial condition deviation, can bring unexpected consequences to the actual systems and will severely degrade the control system performance. Consequently, it is of prominent importance to compensate uncertainties in control design.

To eliminate the influence of uncertainties, the radial basis function (RBF) neural network and fuzzy RBF neural network are respectively employed in refs. [14] and [15], and a compensator using a nonlinear disturbance observer is designed in ref. [16]. In ref. [17], a signal compensation-based robust control method is proposed. However, these methods only consider the matched friction in the actuated link. In ref. [18], a constraint-following-based robust control scheme is developed to cope with the mismatched uncertainty. However, the upper bounds of uncertainties need to be known beforehand. For the uncertainties such as the dynamic friction, modeling errors that exist in the actual Pendubot system, the upper bound is usually unknown. Consequently, it is necessary to design a controller that can deal with uncertainties with unknown upper bound so as to achieve the effective control of the Pendubot system.

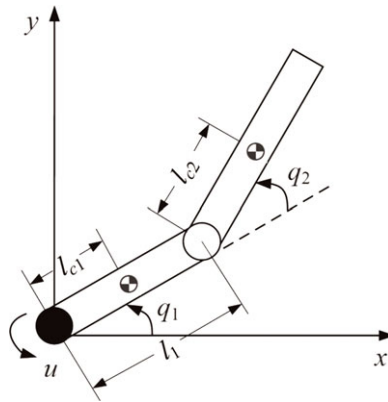


Figure 1. Diagram of the Pendubot.

This paper proposes an adaptive robust constraint-following control approach for the Pendubot system subjects to matched and mismatched uncertainty. To begin with, a nominal control is investigated for the Pendubot without uncertainty. Then, the uncertainty is specially decomposed into the matched portion and the unmatched portion. Based on that, an adaptive robust control law is devised to tackle initial condition deviation and uncertainty. By using the Lyapunov approach, the developed approach is proved to be both uniformly bounded and uniformly ultimately bounded, rendering approximate constraint-following to the Pendubot system subjects to initial condition deviation and uncertainty. Finally, simulation and experimental results are presented, demonstrating the good tracking accuracy and robustness of the proposed approach.

The major contributions of the research are the following. First, the robust control problem of the Pendubot subjects to matched and unmatched uncertainties is formulated as a constraint-following control problem with reduced-dimension equality constraints. Second, a robust constraint-following control method is proposed with a leakage-type adaptive law. Unlike the existing methods requiring the information of the uncertainty bound, the proposed approach removes this limitation and can well tackle uncertainties with unknown bounds. Third, the closed-loop Pendubot system is proved to be both uniformly bounded and uniformly ultimately bounded under the action of the proposed approach.

The remainder of the study is organized as follows. The task to be addressed is formulated in Section 2. Section 3 discusses the adaptive robust constraint-following control design. Section 4 presents the stability analysis. Simulation results are provided and discussed in Section 5. The paper is then concluded in Section 6.

2. Constraint-following task formulation

2.1. Dynamics

The schematic of the Pendubot is shown in Fig. 1, where m_1 (m_2) stands for the mass of link 1 (link 2), q_1 denotes the angle of link 1 relative to the horizontal axis, q_2 refers to the angle of link 2 relative to link 1, l_1 (l_2) is the length of link 1 (link 2), l_{c1} (l_{c2}) denotes the distance from the centroid to the connection point of link 1 (link 2), and I_1 (I_2) is the moment of inertia of link 1 (link 2). For simplicity, we introduce five parameters: $\theta_1 = m_1 l_{c1}^2 + m_2 l_1^2 + I_1$, $\theta_2 = m_2 l_{c2}^2 + I_2$, $\theta_3 = m_2 l_1 l_{c2}$, $\theta_4 = m_1 l_{c1} + m_2 l_1$, $\theta_5 = m_2 l_{c2}$.

According to ref. [19], the dynamics of the Pendubot with uncertainty can be obtained as

$$M(q)\ddot{q} + C(q, \dot{q})\dot{q} + G(q) + F(q, \dot{q}) = B\tau, \tag{1}$$

$$\begin{aligned}
 M(q) &= \begin{bmatrix} \theta_1 + \theta_2 + 2\theta_3 \cos q_2 & \theta_2 + \theta_3 \cos q_2 \\ \theta_2 + \theta_3 \cos q_2 & \theta_2 \end{bmatrix}, \\
 C(q, \dot{q}) &= \begin{bmatrix} -\theta_3 \dot{q}_2 & -\theta_3 (\dot{q}_2 + \dot{q}_1) \\ \theta_3 \dot{q}_1 & 0 \end{bmatrix} \sin q_2, \\
 G(q) &= \begin{bmatrix} \theta_4 g \cos(q_1) + \theta_5 g \cos(q_1 + q_2) \\ \theta_5 g \cos(q_1 + q_2) \end{bmatrix}, \\
 F(\dot{q}) &= \begin{bmatrix} f_1(\dot{q}) \\ f_2(\dot{q}) \end{bmatrix}, \quad B = \begin{bmatrix} 1 \\ 0 \end{bmatrix},
 \end{aligned}$$

where $q = [q_1 \ q_2]^T$ and $\dot{q} = [\dot{q}_1 \ \dot{q}_2]^T$ represent the angle vector and angle velocity vector, respectively, $M(q)$ is the symmetric positive definite inertia matrix, $C(q, \dot{q})$ denotes the centripetal and Coriolis torque vector, $G(q)$ stands for the gravitational torque vector, $F(q, \dot{q})$ is the system uncertainty, and τ denotes the input torque applied to link 1.

2.2. Constraints

The control goal is to stabilize both link 1 and link 2 of the Pendubot toward the desired vertical upright position. However, due to the underactuated Pendubot system exhibits nonholonomic constraint, it is impossible to design a stabilizing controller that can render both q_1 and q_2 converging to their target position q_{1d} , q_{2d} , with arbitrary independent convergence curves. These curves may be conflicting with the inherent dynamic coupling, since there is a strong nonlinear coupling between q_1 and q_2 . To solve this, the control objective for the dynamical system (1) is formulated as a constraint-following control problem with the constraint defined as follows between two states as shown in the following lemma.

$$\dot{s} + \zeta s = -\frac{2\eta}{\pi} \arctan(s), \tag{2}$$

with

$$s = \lambda(\dot{e}_1 + \lambda_1 e_1) + (\dot{e}_2 + \lambda_2 e_2), \tag{3}$$

$$e_1 = q_1 - q_{1d}, \quad e_2 = q_2 - q_{2d}, \tag{4}$$

where $q_{1d} = \pi/2$, $q_{2d} = 0$, $\zeta, \eta, \lambda, \lambda_1$, and λ_2 are positive constants, and η is arbitrarily small. From (2) to (4), as $t \rightarrow \infty$, $\frac{2\eta}{\pi} \arctan(s)$ will converge to η . Since η is arbitrarily small, from (2), s will infinitely converge to zero, which means that both q_1 and q_2 will arbitrarily converge to their desired positions q_{1d}, q_{2d} .

With (3) and (4), the constraint (2) is rewritten as

$$\begin{aligned}
 &\lambda \ddot{q}_1 + \lambda \lambda_1 \dot{q}_1 + \ddot{q}_2 + \lambda_2 \dot{q}_2 + \zeta [\lambda \dot{q}_1 + \lambda \lambda_1 (q_1 - \pi/2) + \dot{q}_2 + \lambda_2 q_2] \\
 &= -\frac{2\eta}{\pi} \arctan(\lambda \dot{q}_1 + \lambda \lambda_1 (q_1 - \pi/2) + \dot{q}_2 + \lambda_2 q_2).
 \end{aligned} \tag{5}$$

Remark 1. Obviously, the RHS of (5) is unintegrable, therefore, (5) is a nonholonomic constraint. When $t \rightarrow \infty$, $-\frac{2\eta}{\pi} \arctan(\lambda \dot{q}_1 + \lambda \lambda_1 (q_1 - \frac{\pi}{2}) + \dot{q}_2 + \lambda_2 q_2)$ will converge to an arbitrarily small constant η (but not equal to zero). As a consequence, $\lambda \dot{q}_1 + \lambda \lambda_1 (q_1 - \frac{\pi}{2}) + \dot{q}_2 + \lambda_2 q_2$ will converge to zero, hence $\dot{q}_1 + \lambda_1 (q_1 - \frac{\pi}{2})$ and $\dot{q}_2 + \lambda_2 q_2$ will converge to zero simultaneously, indicating both q_1 and q_2 will converge to their desired points. This shows that the motor torque can control both the actuated link angle and underactuated link angle to approximately follow their desired positions.

Integrating (5) from 0 to t , we obtain

$$\begin{aligned} & \lambda(\dot{q}_1 - \dot{q}_1(0)) + \lambda\lambda_1(q_1 - q_1(0)) + (\dot{q}_2 - \dot{q}_2(0)) + \lambda_2(q_2 - q_2(0)) + \varsigma\lambda(q_1 - q_1(0)) \\ & + \varsigma\lambda\lambda_1 \int_0^t (q_1 - \pi/2)d\tau + \varsigma(q_2 - q_2(0)) + \varsigma\lambda_2 \int_0^t q_2d\tau \\ & = -\frac{2\eta}{\pi} \int_0^t \arctan(\lambda\dot{q}_1 + \lambda\lambda_1(q_1 - \pi/2) + \dot{q}_2 + \lambda_2q_2)d\tau, \end{aligned} \tag{6}$$

where $q_1(0)$, $q_2(0)$, $\dot{q}_1(0)$, and $\dot{q}_2(0)$ are the initial values of q_1 , q_2 , \dot{q}_1 , and \dot{q}_2 , respectively. Let

$$\begin{aligned} A &= [\lambda \quad 1], \\ b &= -\lambda\lambda_1\dot{q}_1 - \lambda_2\dot{q}_2 - \varsigma[\lambda\dot{q}_1 + \lambda\lambda_1(q_1 - \pi/2) + \dot{q}_2 + \lambda_2q_2] \\ & \quad - \frac{2\eta}{\pi}\arctan(\lambda\dot{q}_1 + \lambda\lambda_1(q_1 - \pi/2) + \dot{q}_2 + \lambda_2q_2), \\ c &= \lambda\dot{q}_1(0) - \lambda\lambda_1(q_1 - q_1(0)) + \dot{q}_2(0) - \lambda_2(q_2 - q_2(0)) \\ & \quad - \varsigma\lambda(q_1 - q_1(0)) - \varsigma(q_2 - q_2(0)) - \varsigma\lambda\lambda_1 \int_0^t (q_1 - \pi/2)d\tau \\ & \quad - \varsigma\lambda_2 \int_0^t q_2d\tau - \frac{2\eta}{\pi} \int_0^t \arctan(\lambda\dot{q}_1 + \lambda\lambda_1(q_1 - \pi/2) + \dot{q}_2 + \lambda_2q_2)d\tau, \end{aligned} \tag{7}$$

then (5) and (6) can be rewritten as

$$\begin{aligned} A\dot{q} &= c, \\ A\ddot{q} &= b. \end{aligned} \tag{8}$$

3. Adaptive robust control design

3.1. Uncertainty decomposition

The Pendubot dynamics (1) contains both matched and mismatched uncertainties. Due to the lack of control input, mismatched uncertainties bring great obstacle to the control design. In view of this, the uncertainty F is specially divided into the matched part $B(q, \dot{q})\hat{F}(q, \dot{q})$, which is in the range space of $B(q, \dot{q})$, and the mismatched part $\Delta\tilde{F}(q, \dot{q})$, which is in the bull space of $B(q, \dot{q})$, that is,

$$F(q, \dot{q}) = B(q, \dot{q})\hat{F}(q, \dot{q}) + \Delta\tilde{F}(q, \dot{q}). \tag{9}$$

Let $D = M^{-1}$, then we have

$$AM^{-1}B = ADB = \frac{\lambda\theta_2}{\theta_1\theta_2 - \theta_3^2\cos^2q_2} > 0, \tag{10}$$

therefore ADB is invertible.

To exploit the constraint (8), we introduce an orthogonal decomposition approach [20] and specially decompose the uncertainty F based on the constraint matrix A and the parameter matrixes B, D . Based on that, the decomposition is specified as

$$\begin{aligned} \hat{F}(q, \dot{q}) &= (A(q, \dot{q})D(q, \dot{q})B(q, \dot{q}))^{-1}A(q, \dot{q})D(q, \dot{q})F(q, \dot{q}), \\ \Delta\tilde{F}(q, \dot{q}) &= F(q, \dot{q}) - B(q, \dot{q})\hat{F}(q, \dot{q}). \end{aligned} \tag{11}$$

From (9) and (11),

$$A(q, \dot{q})D(q, \dot{q})\Delta\tilde{F}(q, \dot{q}) \equiv 0. \tag{12}$$

The above decomposition arranges the unmatched portion $\Delta\tilde{F}(q, \dot{q})$ to be in the null space of $A(q, \dot{q})D(q, \dot{q})$. Thus, $\Delta\tilde{F}(q, \dot{q})$ will not affect the constraint-following performance. This allows the control to be designed without considering the unmatched part and just based on the matched one, which will be used in later derivation.

3.2. Control design

Before the control design of the Pendubot system (1), we make the following two assumptions.

Assumption 1: *There is a positive constant $\underline{\lambda}$ such that*

$$ADBB^T DA^T \geq \underline{\lambda}. \tag{13}$$

Remark 2. In fact, Assumption 1 means that the minimum of ADB always has a finite distance from 0. Since we already have $ADB > 0$, it is reasonable to make this assumption.

Assumption 2: *There is an unknown constant vector $\alpha \in (0, \infty)^k$ and a known function $\Pi(q, \dot{q}) : \mathbf{R}^2 \times \mathbf{R}^2 \rightarrow \mathbf{R}^k$ such that for all $(q, \dot{q}) \in \mathbf{R}^2 \times \mathbf{R}^2$,*

$$\max\|\hat{F}(q, \dot{q})\| \leq \alpha^T \Pi(q, \dot{q}), \tag{14}$$

where the function $\alpha^T \Pi(q, \dot{q})$ refers to the uncertainty bound and the unknown vector α depends on the bound of the uncertainty $\hat{F}(q, \dot{q})$.

Remark 3. In a sense, what Assumption 2 does is the parameterization of the worst effect of the uncertainty $\hat{F}(q, \dot{q})$, which will be further elaborated in the proof of Theorem 1.

In practice, it is an arduous task to acquire the specific value of α , since it may be related to the bounding set. As a result, the following leakage-type adaptive law is designed

$$\dot{\hat{\alpha}} = \kappa_1 \Pi(q, \dot{q}) \|\hat{\beta}(q, \dot{q})\| - \kappa_2 \hat{\alpha}, \tag{15}$$

where $\kappa_1 > 0$ and $\kappa_2 > 0$ are constants, $\hat{\alpha} \in \mathbf{R}^k$ is the estimated value of α , $\hat{\alpha}_i(t_0) > 0, i = 1, \dots, k$.

Remark 4. According to (15), $\hat{\alpha}_i(t) > 0$ for all $t \geq t_0$. This is because the first term $\kappa_1 \Pi(q, \dot{q}) \|\hat{\beta}(q, \dot{q})\|$ on the right half side of (15) is always non-negative and the second term $-\kappa_2 \hat{\alpha}$ alone will render an exponentially decaying (to zero) solution from above. The leakage item $-\kappa_2 \hat{\alpha}$ in (15) prevents the constantly increase of $\hat{\alpha}$.

Then, the adaptive robust constraint-following control law is proposed as follows:

$$\tau = p_1(q, \dot{q}) + p_2(q, \dot{q}) + p_3(\hat{\alpha}, q, \dot{q}), \tag{16}$$

where

$$p_1(q, \dot{q}) = (A(q, \dot{q})D(q, \dot{q})B(q, \dot{q}))^{-1} [b(q, \dot{q}) + A(q, \dot{q})D(q, \dot{q})(C(q, \dot{q})\dot{q} + G(q, \dot{q}))], \tag{17}$$

$$p_2(q, \dot{q}) = -\kappa \hat{\beta}(q, \dot{q}), \tag{18}$$

$$p_3(\hat{\alpha}, q, \dot{q}) = -\gamma(\hat{\alpha}, q, \dot{q}) \mu(\hat{\alpha}, q, \dot{q}) \hat{\alpha}^T \Pi(q, \dot{q}), \tag{19}$$

where $\kappa > 0$ is a constant,

$$\hat{\beta}(q, \dot{q}) = B^T(q, \dot{q})D(q, \dot{q})A^T(q, \dot{q})\beta(q, \dot{q}), \tag{20}$$

$$\beta(q, \dot{q}) = A(q, \dot{q})\dot{q} - c(q, \dot{q}), \tag{21}$$

$$\mu(\hat{\alpha}, q, \dot{q}) = \hat{\beta}(q, \dot{q}) \hat{\alpha}^T \Pi(q, \dot{q}), \tag{22}$$

$$\gamma(\hat{\alpha}, q, \dot{q}) = \begin{cases} \frac{1}{\|\mu(\hat{\alpha}, q, \dot{q})\|}, & \text{if } \|\mu(\hat{\alpha}, q, \dot{q})\| > \varepsilon \\ \frac{1}{\varepsilon}, & \text{if } \|\mu(\hat{\alpha}, q, \dot{q})\| \leq \varepsilon \end{cases}, \tag{23}$$

where $\varepsilon > 0$ is a given small constant, and $\hat{\alpha}$ is determined by the adaptive law in (15).

Remark 5. Different from ref. [17], which only considers the matched uncertainty, this paper considers both matched and unmatched uncertainty. In refs. [18, 20], the parameter α is assumed to be known. However, in this paper, α is unknown and is estimated using the leakage-type adaptive law in (15).

4. Stability analysis

Theorem 1. Consider the Pendubot system (1) subjects to Assumptions 1–2 and let $\delta(t) := [\beta^T(q(t), \dot{q}(t)) (\hat{\alpha}(t) - \alpha)^T]^T$, under the action of the adaptive robust control (16)–(23), the Pendubot system has the following performance:

- (i) *Uniformly bounded:* For any $r > 0$, there exists a $d(r) < \infty$ such that for all $t \geq t_0$, if $\|\delta(t_0)\| \leq r$, then $\|\delta(t)\| \leq r$;
- (ii) *Uniformly ultimately bounded:* For any $r > 0$ with $\|\delta(t_0)\| \leq r$, there is $\underline{d} > 0$ such that for any $\bar{d} > \underline{d}$, $\|\delta(t)\| \leq \bar{d}$ as $t \geq t_0 + T(\bar{d}, r)$, where $0 \leq T(\bar{d}, r) < \infty$.

Proof: Choose the Lyapunov candidate function as

$$V(\beta, \hat{\alpha} - \alpha) = \beta^T \beta + \kappa_1^{-1} (\hat{\alpha} - \alpha)^T (\hat{\alpha} - \alpha). \tag{24}$$

Then, the derivative of V is represented as

$$\dot{V} = 2\beta^T \dot{\beta} + 2\kappa_1^{-1} (\hat{\alpha} - \alpha)^T \dot{\hat{\alpha}}. \tag{25}$$

Next, we will make a separate analysis of each item. For the first item of (25),

$$\begin{aligned} 2\beta^T \dot{\beta} &= 2\beta^T (A\ddot{q} - b) \\ &= 2\beta^T \{AM^{-1}[(-C\dot{q} - G - F) + B(p_1 + p_2 + p_3)] - b\} \\ &= 2\beta^T \{AD[(-C\dot{q} - G) + (Bp_1 + Bp_2) - F + Bp_3] - b\}. \end{aligned} \tag{26}$$

In view of p_1 in (17), we can obtain

$$AD[(-C\dot{q} - G) + Bp_1] - b = 0. \tag{27}$$

From the decomposition in (9) and (12), we have

$$\begin{aligned} ADF &= ADB\hat{F} + AD\Delta\tilde{F} \\ &= ADB\hat{F} + 0 \\ &= ADB\hat{F}. \end{aligned} \tag{28}$$

Introducing (27) and (28) into (26), we have

$$2\beta^T \dot{\beta} = -2\beta^T ADB\hat{F} + 2\beta^T ADBp_2 + 2\beta^T ADBp_3. \tag{29}$$

From (14) and (20), we obtain

$$\begin{aligned} -2\beta^T ADB\hat{F} &\leq 2\|B^T D A^T \beta\| \|\hat{F}\| \\ &\leq 2\|\hat{\beta}\| \alpha^T \Pi(q, \dot{q}). \end{aligned} \tag{30}$$

With (18), we have

$$2\beta^T ADBp_2 = 2\beta^T ADB(-\kappa B^T DA^T \beta). \tag{31}$$

According to the Rayleigh’s principle and Assumption 1,

$$\begin{aligned} 2\beta^T ADB(-\kappa B^T DA^T \beta) &= -2\kappa\beta^T (ADBB^T DA^T)\beta \\ &\leq -2\kappa\underline{\lambda}\|\beta\|^2. \end{aligned} \tag{32}$$

Combining (31) and (32), we can get

$$2\beta^T ADBp_2 \leq -2\kappa\underline{\lambda}\|\beta\|^2. \tag{33}$$

From (19) and (22), we have

$$\begin{aligned} 2\beta^T ADBp_3 &= 2\beta^T ADB(-\gamma\mu\hat{\alpha}^T \Pi(q, \dot{q})) \\ &= -2\gamma\beta^T ADB\mu\hat{\alpha}^T \Pi(q, \dot{q}) \\ &= -2\gamma\|\mu\|^2. \end{aligned} \tag{34}$$

By (23), for $\|\mu\| > \varepsilon$,

$$-2\gamma\|\mu\|^2 = -2\|\mu\|. \tag{35}$$

If $\|\mu\| \leq \varepsilon$, then

$$-2\gamma\|\mu\|^2 = -2\frac{\|\mu\|^2}{\varepsilon}. \tag{36}$$

With (29), (30), (33), (34), and (35), for $\|\mu\| > \varepsilon$,

$$\begin{aligned} 2\beta^T \dot{\beta} &\leq -2\kappa\underline{\lambda}\|\beta\|^2 - 2\|\mu\| + 2\|\hat{\beta}\|\alpha^T \Pi(q, \dot{q}) \\ &= -2\kappa\underline{\lambda}\|\beta\|^2 - 2\|\hat{\beta}\|\hat{\alpha}^T \Pi(q, \dot{q}) + 2\|\hat{\beta}\|\alpha^T \Pi(q, \dot{q}) \\ &= -2\kappa\underline{\lambda}\|\beta\|^2 + 2\|\hat{\beta}\|(\alpha - \hat{\alpha})^T \Pi(q, \dot{q}). \end{aligned} \tag{37}$$

For $\|\mu\| \leq \varepsilon$, with (22) and (36),

$$\begin{aligned} 2\beta^T \dot{\beta} &\leq -2\kappa\underline{\lambda}\|\beta\|^2 - 2\frac{\|\mu\|^2}{\varepsilon} + 2\|\hat{\beta}\|\alpha^T \Pi(q, \dot{q}) \\ &= -2\kappa\underline{\lambda}\|\beta\|^2 - 2\frac{\|\mu\|^2}{\varepsilon} + 2\|\hat{\beta}\|\hat{\alpha}^T \Pi(q, \dot{q}) - 2\|\hat{\beta}\|\hat{\alpha}^T \Pi(q, \dot{q}) + 2\|\hat{\beta}\|\alpha^T \Pi(q, \dot{q}) \\ &\leq -2\kappa\underline{\lambda}\|\beta\|^2 - 2\frac{\|\mu\|^2}{\varepsilon} + 2\|\mu\| + 2\|\hat{\beta}\|(\alpha - \hat{\alpha})^T \Pi(q, \dot{q}) \\ &= -2\kappa\underline{\lambda}\|\beta\|^2 - 2\left(\frac{\|\mu\|^2}{\varepsilon} - \|\mu\|\right) + 2\|\hat{\beta}\|(\alpha - \hat{\alpha})^T \Pi(q, \dot{q}) \\ &\leq -2\kappa\underline{\lambda}\|\beta\|^2 + 2\frac{1}{4/\varepsilon} + 2\|\hat{\beta}\|(\alpha - \hat{\alpha})^T \Pi(q, \dot{q}) \\ &= -2\kappa\underline{\lambda}\|\beta\|^2 + \frac{\varepsilon}{2} + 2\|\hat{\beta}\|(\alpha - \hat{\alpha})^T \Pi(q, \dot{q}). \end{aligned} \tag{38}$$

The first equality above holds simply due to the addition and subtraction of an item simultaneously. From (37) and (38), for all $\|\mu\|$,

$$2\beta^T \dot{\beta} \leq -2\kappa\underline{\lambda}\|\beta\|^2 + \frac{\varepsilon}{2} + 2\|\hat{\beta}\|(\alpha - \hat{\alpha})^T \Pi(q, \dot{q}). \tag{39}$$

For the last term of (25), by utilizing the adaptive law designed in (15), one has

$$\begin{aligned}
 2\kappa_1^{-1}(\hat{\alpha} - \alpha)^T \dot{\hat{\alpha}} &= 2\kappa_1^{-1}(\hat{\alpha} - \alpha)^T (\kappa_1 \Pi(q, \dot{q}) \|\hat{\beta}\| - \kappa_2 \hat{\alpha}) \\
 &= 2(\hat{\alpha} - \alpha)^T \Pi(q, \dot{q}) \|\hat{\beta}\| - 2\kappa_1^{-1}(\hat{\alpha} - \alpha)^T \kappa_2 \hat{\alpha} \\
 &= 2(\hat{\alpha} - \alpha)^T \Pi(q, \dot{q}, t) \|\hat{\beta}\| - 2\kappa_1^{-1} \kappa_2 (\hat{\alpha} - \alpha)^T (\hat{\alpha} - \alpha + \alpha) \\
 &= 2(\hat{\alpha} - \alpha)^T \Pi(q, \dot{q}) \|\hat{\beta}\| - 2\kappa_1^{-1} \kappa_2 (\hat{\alpha} - \alpha)^T (\hat{\alpha} - \alpha) - 2\kappa_1^{-1} \kappa_2 (\hat{\alpha} - \alpha)^T \alpha \\
 &\leq 2(\hat{\alpha} - \alpha)^T \Pi(q, \dot{q}) \|\hat{\beta}\| - 2\kappa_1^{-1} \kappa_2 \|\hat{\alpha} - \alpha\|^2 + 2\kappa_1^{-1} \kappa_2 \|\hat{\alpha} - \alpha\| \|\alpha\|.
 \end{aligned} \tag{40}$$

With (39) and (40), (25) becomes (by using $\|\delta\|^2 = \|\beta\|^2 + \|\hat{\alpha} - \alpha\|^2$)

$$\begin{aligned}
 \dot{V} &\leq -2\kappa \underline{\lambda} \|\beta\|^2 + \frac{\varepsilon}{2} - 2\kappa_1^{-1} \kappa_2 \|\hat{\alpha} - \alpha\|^2 + 2\kappa_1^{-1} \kappa_2 \|\hat{\alpha} - \alpha\| \|\alpha\| \\
 &\leq -\underline{\kappa}_1 \|\delta\|^2 + \underline{\kappa}_2 \|\delta\| + \underline{\kappa}_3,
 \end{aligned} \tag{41}$$

where

$$\begin{aligned}
 \underline{\kappa}_1 &= \min\{2\kappa \underline{\lambda} (1 + \rho_\Omega), 2\kappa_1^{-1} \kappa_2 (1 + \rho_\Omega)\}, \\
 \underline{\kappa}_2 &= 2\kappa_1^{-1} \kappa_2 (1 + \rho_\Omega) \|\alpha\|, \\
 \underline{\kappa}_3 &= (1 + \rho_\Omega) \varepsilon / 2.
 \end{aligned} \tag{42}$$

Therefore, by refs. [21] and [22], the uniform boundedness can be concluded with

$$d(r) = \begin{cases} \sqrt{\frac{\gamma_M}{\gamma_m}} R, & \text{if } r \leq R, \\ \sqrt{\frac{\gamma_M}{\gamma_m}} r, & \text{if } r > R, \end{cases} \quad R = \frac{1}{2\underline{\kappa}_1} \left(\underline{\kappa}_2 + \sqrt{\underline{\kappa}_2^2 + 4\underline{\kappa}_1 \underline{\kappa}_3} \right), \tag{43}$$

where

$$\begin{aligned}
 \gamma_m &= \min\{\lambda_{\min}(P), 2\underline{\kappa}_1^{-1} (1 + \rho_\Omega)\}, \\
 \gamma_M &= \max\{\lambda_{\max}(P), 2\underline{\kappa}_1^{-1} (1 + \rho_\Omega)\}.
 \end{aligned} \tag{44}$$

Moreover, uniform ultimate boundedness follows with

$$\underline{d} = \sqrt{\frac{\gamma_M}{\gamma_m}} R, \tag{45}$$

$$T(\bar{d}, r) = \begin{cases} 0, & \text{if } r \leq \bar{d} \sqrt{\frac{\gamma_m}{\gamma_M}}, \\ \frac{\gamma_M r^2 - (\gamma_m^2 / \gamma_M) \bar{d}^2}{\underline{\kappa}_1 \bar{d}^2 (\gamma_m / \gamma_M) - \underline{\kappa}_2 \bar{d} (\gamma_m / \gamma_M)^{1/2} - \underline{\kappa}_3}, & \text{otherwise.} \end{cases} \tag{46}$$

□

5. Simulation results

To verify the effectiveness and feasibility of the proposed approach, simulation results are provided in this section. Throughout the simulations, the physical parameters of the Pendubot are chosen as: $m_1=0.09$ kg, $m_2=0.73$ kg, $l_1=0.15$ m, $l_{c1}=0.09$ m, $l_{c2}=0.08$ m, $I_1 = 0.0073$ kg · m², $I_2 = 0.0001$ kg · m²,

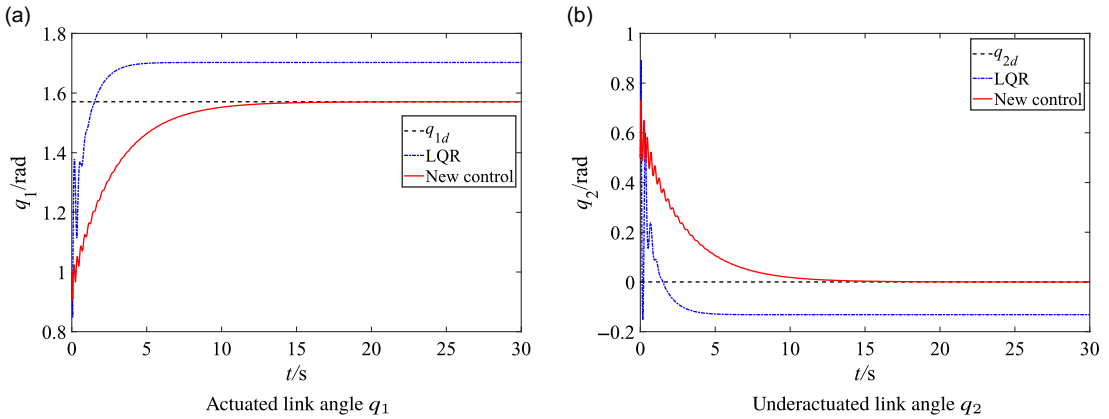


Figure 2. Comparison of the outputs under LQR and the proposed control.

$g = 9.8 \text{ kg/m}^2$. The initial conditions of the Pendubot system are: $q_1(0) = 1 \text{ rad}$, $q_2(0) = 0.5 \text{ rad}$, $\dot{q}_1(0) = \dot{q}_2(0) = 0 \text{ rad/s}$. All the simulations are performed in Matlab by using the ode45 solver.

The standard linear quadratic regulator (LQR) is selected for comparison. The most common robustness of LQR can be attributed to a one-half gain reduction, an infinite gain amplification, or a phase error of positive or negative sixty degrees in the input channel. Furthermore, the robustness of LQR includes uncertainty in the real coefficients of the linearized model and certain nonlinearities such as switching and saturation.

According to (16), we choose

$$\Pi(q, \dot{q}) = (\|\dot{e}\| + 1)^2 + (\|e\| + 1)^2, \tag{47}$$

and the adaptive law (15) is given by

$$\begin{aligned} \dot{\hat{\alpha}} = & \kappa_1 \left((\|\dot{e}\| + 1)^2 + (\|e\| + 1)^2 \right) \left| \frac{\theta_2}{\theta_1\theta_2 - \theta_3^2 \cos^2 q_2} \{ \lambda(\dot{q}_1 - \dot{q}_1(0)) + \lambda\lambda_1(q_1 - q_1(0)) + (\dot{q}_2 - \dot{q}_2(0)) \right. \\ & + \lambda_2(q_2 - q_2(0)) + \varsigma\lambda(q_1 - q_1(0)) + \varsigma\lambda\lambda_1 \int_0^t (q_1 - \pi/2) d\tau + \varsigma(q_2 - q_2(0)) + \varsigma\lambda_2 \int_0^t q_2 d\tau \\ & \left. + \frac{2\eta}{\pi} \int_0^t \arctan(\lambda\dot{q}_1 + \lambda\lambda_1(q_1 - \pi/2) + \dot{q}_2 + \lambda_2 q_2) d\tau \right\} - \kappa_2 \hat{\alpha}, \end{aligned} \tag{48}$$

where $\hat{\alpha}(t_0) > 0$. Next, three sets of simulations will be carried out.

5.1. Matched constant uncertainty

Consider the Pendubot system with matched constant uncertainty (there are constant disturbances in the actuated link), that is, $f_1 = 2, f_2 = 0$, the parameters of constraints are chosen as: $\lambda = 2.25, \lambda_1 = 0.55, \lambda_2 = 0.7, \varsigma = 2, \eta = 0.001$. Obviously, the above initial condition does not satisfy the constraint (2). Hence, we use $p_1 + p_2$ for the control, and the control parameter $\kappa = 2$. The parameters of LQR are chosen as $Q = I, R = 1$.

Figure 2 depicts the output angles of the Pendubot under the LQR control and the proposed control. As seen from Fig. 2, under the action of LQR, the Pendubot system can converge quickly; however, both the actuated and unactuated link angles suffer certain salient deviation from the target position. Comparing to LQR, the proposed control has better control performance. After some time, both the actuated and unactuated links achieve each control goal simultaneously and the positioning error is small enough in contrast with the LQR control. This is mainly due to the compensatory effect of p_2 . To demonstrate this point, the comparative simulation results of p_1 and $p_1 + p_2$ are given in Fig. 3.

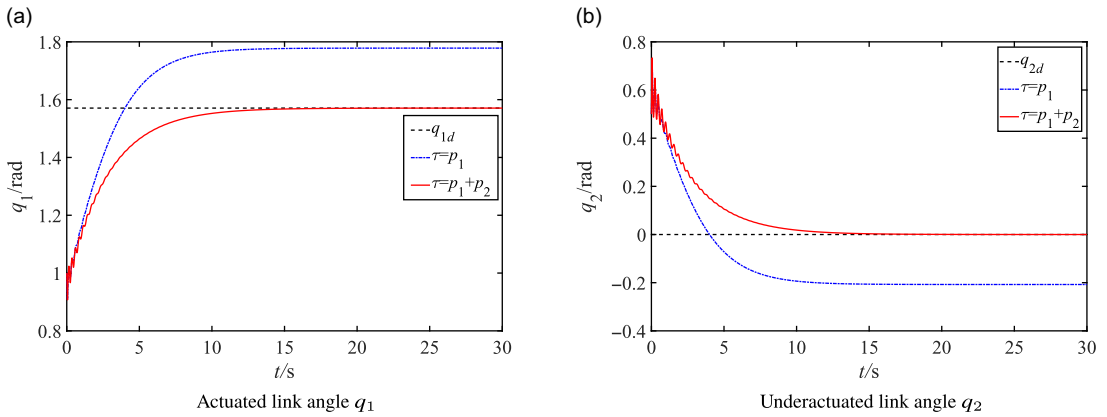


Figure 3. Comparison of the Pendubot outputs under p_1 and $p_1 + p_2$.

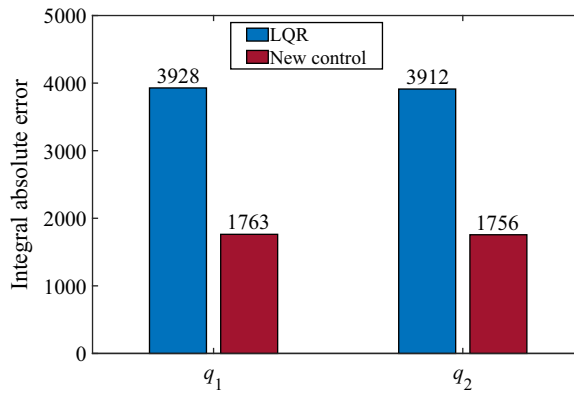


Figure 4. The integral absolute error.

Figures 4, 5, and 6 provide the integral absolute error (IAE) ($\int_0^{t_f} |q_1 - q_{1d}| dt, \int_0^{t_f} |q_2 - q_{2d}| dt$, where $[0, t_f]$ is the considered interval of time), the maximal absolute error (MAE) ($\max_{0 \leq t \leq t_f} \{|q_1 - q_{1d}|\}, \max_{0 \leq t \leq t_f} \{|q_2 - q_{2d}|\}$), and the maximal absolute error during the last two seconds (MAE2) ($\max_{t_f - 2 \leq t \leq t_f} \{|q_1 - q_{1d}|\}, \max_{t_f - 2 \leq t \leq t_f} \{|q_2 - q_{2d}|\}$) of q_1 and q_2 , respectively. From Figs. 4, 5, and 6, it can be seen that the values of IAE, MAE, and MAE2 of the proposed control are smaller than that of LQR, which indicates that the system presents better dynamic performance, transient performance, and final tracking accuracy under the action of the method presented in this paper.

5.2. Matched time-varying uncertainty

Considering the nonlinear time-varying friction model in ref. [19], we employ the matched uncertainty F as follows: $f_1 = 4.18(\tanh(1.59\dot{q}_1) - \tanh(3.15\dot{q}_1)) + 0.09\tanh(3.52\dot{q}_1) + 0.021\dot{q}_1, f_2 = 0$. Since there are both uncertainty and initial condition deviation, we adopt the control law $\tau = p_1 + p_2 + p_3$ in (16) and the control parameters are $\kappa = 2, \varepsilon = 0.001, \kappa_1 = 0.02, \kappa_2 = 2$. Figure 7 shows the history of $ADBB^T DA^T$. It can be found that $ADBB^T DA^T$ is not infinitely approaching to zero. Hence, there exists $\underline{\lambda} > 0$ such that Assumption 1 is verified.

The outputs of the Pendubot by LQR and the proposed adaptive robust control are depicted in Fig. 8. In Fig. 9, we also compare the maximal absolute tracking errors of q_1 and q_2 during the last 2 s. It shows that the proposed control has higher final tracking accuracy. The absolute constraint-following

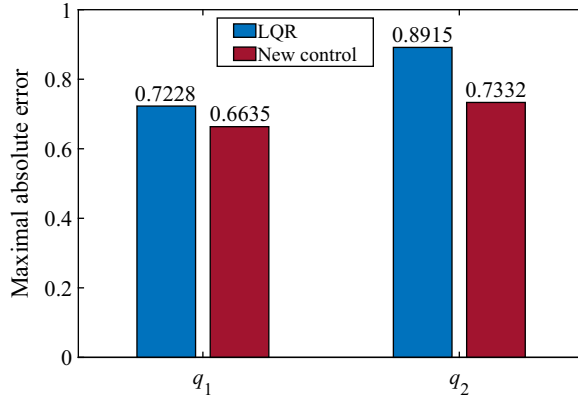


Figure 5. The maximal absolute error.

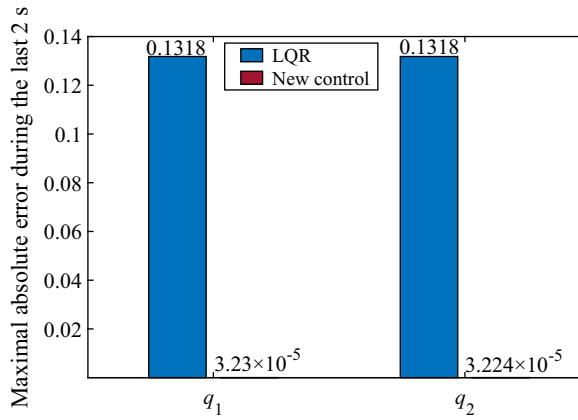


Figure 6. The maximal absolute error during the last 2 s.

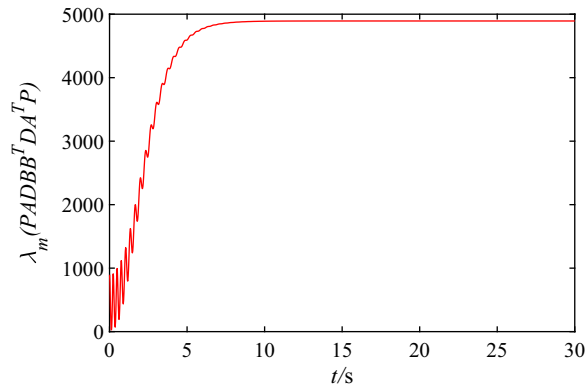


Figure 7. History of $ADBB^T DA^T$.

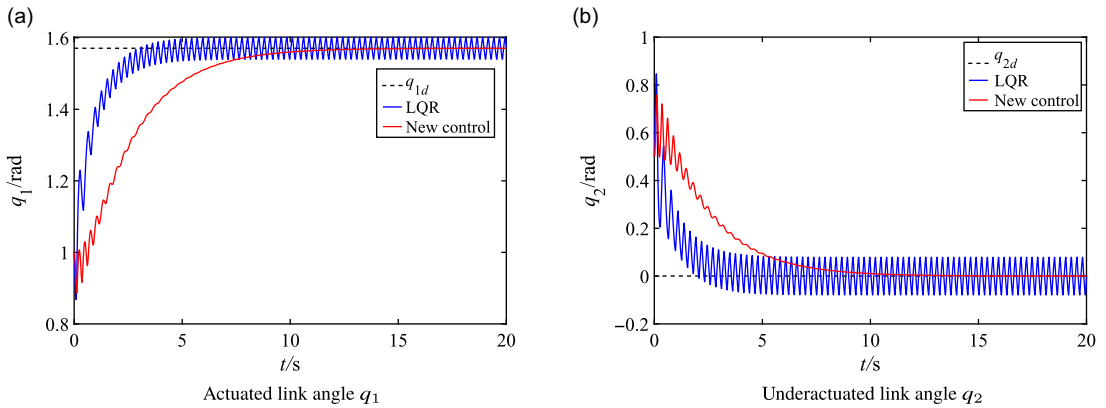


Figure 8. The outputs of the Pendubot.

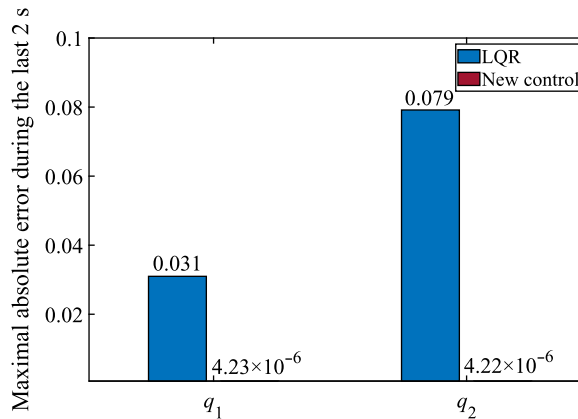


Figure 9. The maximal error during the last 2 s.

errors $|\beta|$ of the conventional LQR and the proposed control are shown in Fig. 10. After some time, the constraint-following error of the developed approach enters a small area near zero, which indicates that $|\beta|$ is uniformly ultimately bounded. Figures 11 and 12 show the accumulative absolute constraint-following error and the control effort, respectively. As seen from Figs. 11 and 12, the proposed method is superior to LQR.

5.3. Matched and unmatched time-varying uncertainty

For the matched and unmatched time-varying uncertainty, we consider the friction both in the actuated link and the unactuated link and choose F as [16]: $f_1 = 4.18(\tanh(1.59\dot{q}_1) - \tanh(3.15\dot{q}_1)) + 0.09\tanh(3.52\dot{q}_1) + 0.021\dot{q}_1$, $f_2 = 4.18(\tanh(1.59\dot{q}_2) - \tanh(3.15\dot{q}_2)) + 0.09\tanh(3.52\dot{q}_2) + 0.021\dot{q}_2$. To handle both uncertainty and initial condition deviation, we use the control law $\tau = p_1 + p_2 + p_3$. The control parameters are the same as last session. Figure 13 shows the history of $ADBB^T DA^T$. It can be found that $ADBB^T DA^T$ is not infinitely close to zero. Hence, there exists $\underline{\lambda} > 0$ such that Assumption 1 is verified.

The outputs of the Pendubot system by the proposed new control are presented in Fig. 14. The constraint-following error $|\beta|$ is given in Fig. 15. We can see that $|\beta|$ enters a small neighborhood of

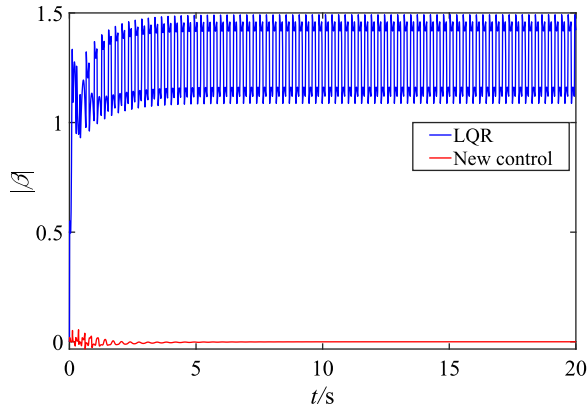


Figure 10. The constraint-following error.

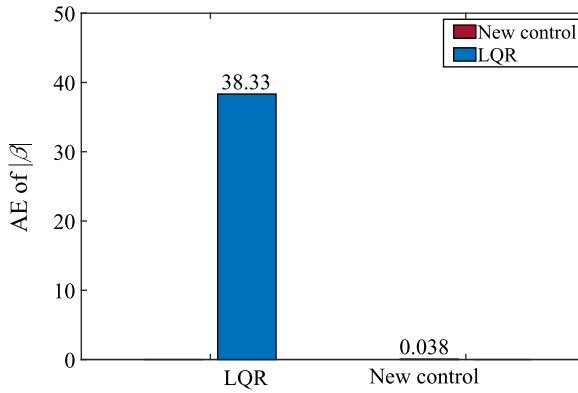


Figure 11. The accumulative absolute error.

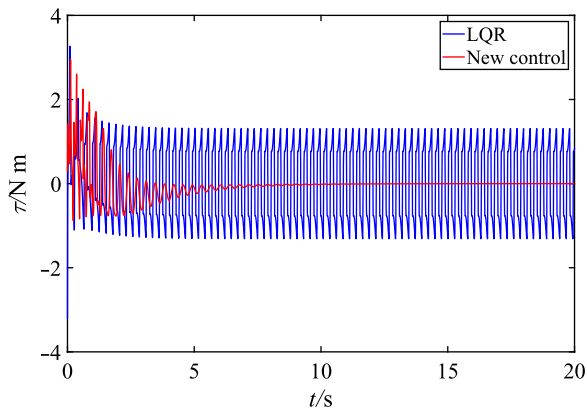


Figure 12. The control input.

zero after some time, which indicates the uniform ultimate boundedness of the constraint-following error. Figure 16 shows the control $p_1, p_2,$ and p_3 .

The above three groups of simulation evidently illustrate that the proposed robust control can effectively eliminate the uncertainty, whether constant or time-varying, matched or unmatched.

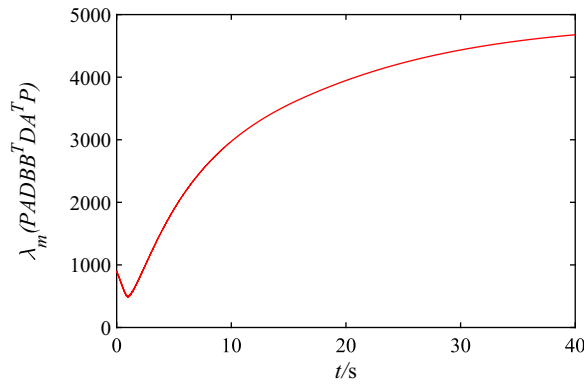


Figure 13. History of $ADBB^T DA^T$ with matched and unmatched uncertainty.

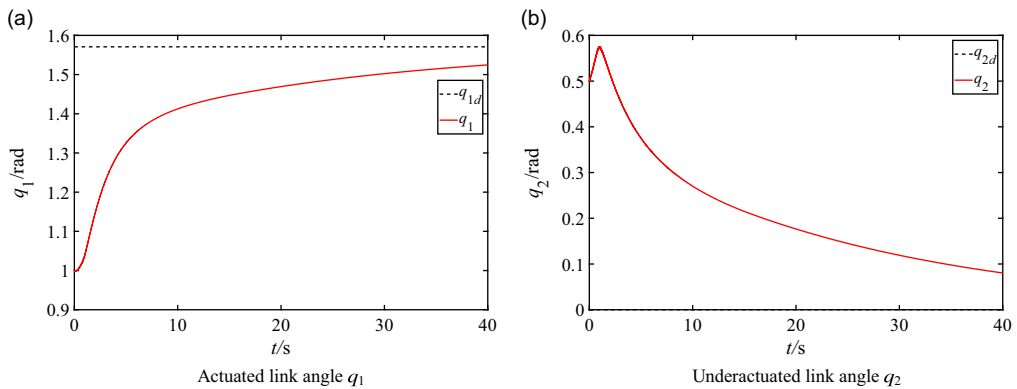


Figure 14. Outputs of the Pendubot with matched and unmatched uncertainties.

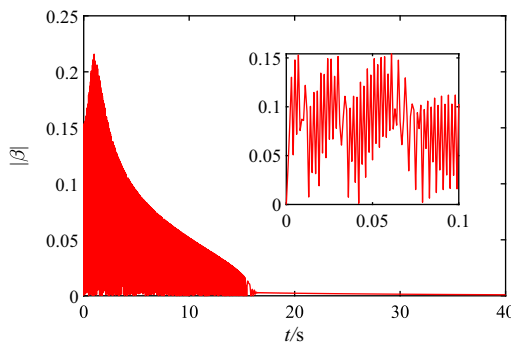


Figure 15. The constraint-following error.

6. Experimental results

To validate the effectiveness of the proposed adaptive robust control method, experiments were carried out on an actual Pendubot system, where there exist matched and unmatched uncertainties. The Pendubot experimental system consists of three parts: a PC monitor, an embedded controller, and the Pendubot system. The Pendubot is driven by a servo motor with rated voltage of 90 V and no-load speed of

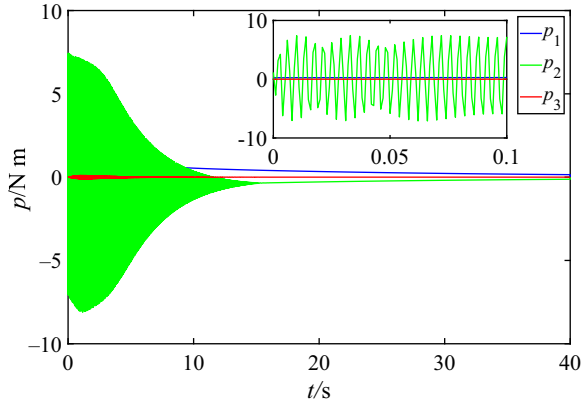


Figure 16. The control input.

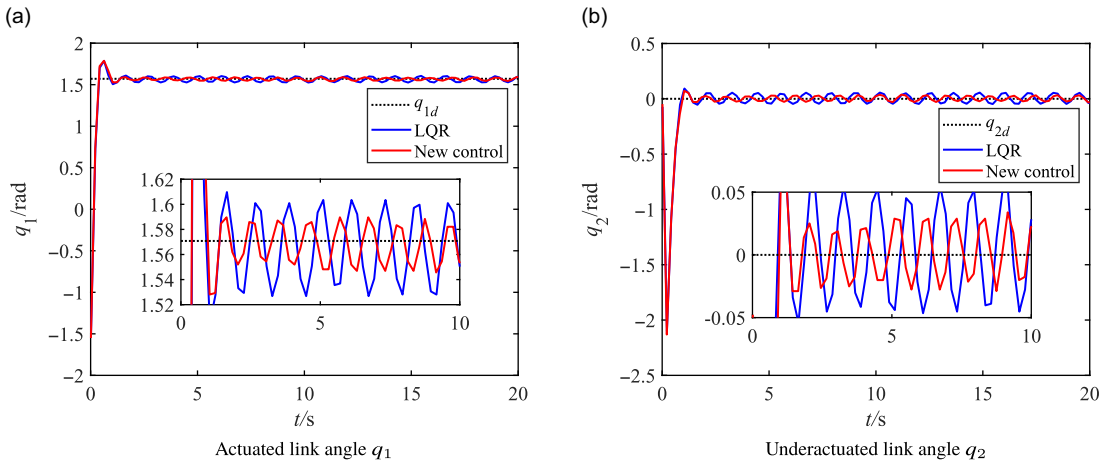


Figure 17. The experimental outputs of the Pendubot.

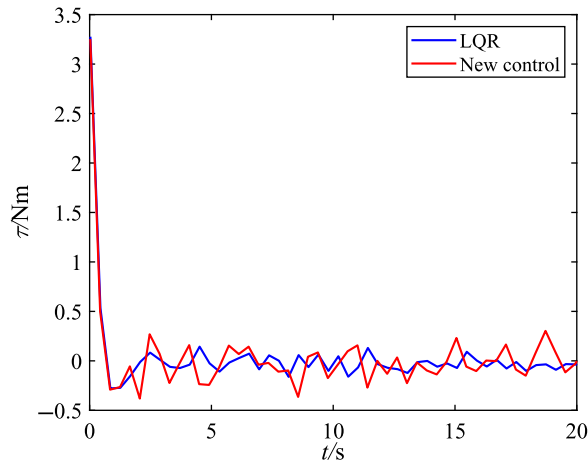


Figure 18. The control input.

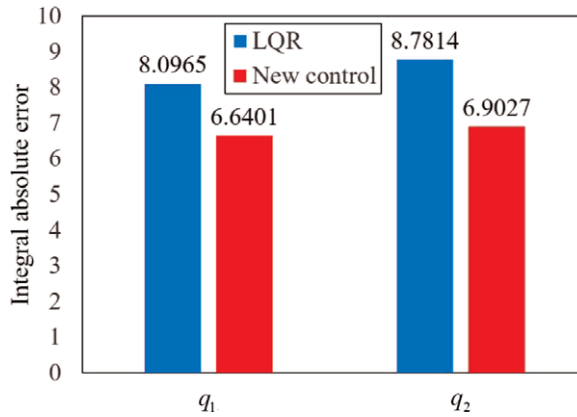


Figure 19. The integral absolute error.

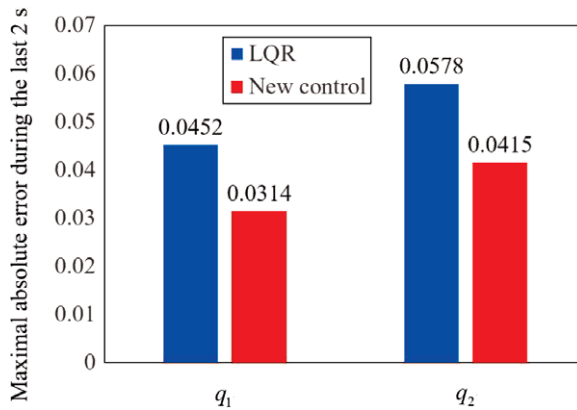


Figure 20. The maximal absolute error during the last 2 s.

2000 r/min. The control algorithm is implemented on the embedded controller with a PowerPC processor running at 1 GHz. The angles of the actuated and unactuated link are measured by two encoders of 1250 pulses per revolution. The parameters of the Pendubot system in (1) are identified as $\theta_1 = 0.0096 \text{ kg} \cdot \text{m}^2$, $\theta_2 = 0.0054 \text{ kg} \cdot \text{m}^2$, $\theta_3 = 0.0046 \text{ kg} \cdot \text{m}^2$, $\theta_4 = 0.0679 \text{ kg} \cdot \text{m}^2$, $\theta_5 = 0.0332 \text{ kg} \cdot \text{m}^2$, and $g = 9.8 \text{ m/s}^2$, and the initial position is $(q_1, q_2, \dot{q}_1, \dot{q}_2) = (-\frac{\pi}{2}, 0, 0, 0)$. The swing-up control adopts the energy-based method [12] and the control parameters are $k_p = 66.35$, $k_D = 9.45$, and $k_E = 1$. The switching conditions are $|q_1 - \pi/2| \leq 0.26$, $|q_2| \leq 0.26$. Furthermore, the proposed method was compared with the traditional LQR method.

The experimental results are shown in Figs. 17 and 18. From Fig. 17, it can be seen that the proposed method effectively decreases the fluctuation and tracking error. Figures 19 and 20 provide the IAE and the MAE2 of q_1 and q_2 , respectively. From Figs. 19 and 20, we can see that the values of IAE and MAE2 of the proposed new control are smaller than that of LQR, indicating that the Pendubot system exhibits better dynamic performance and final tracking accuracy under the proposed new control.

7. Conclusion

We investigate the constraint-following control for the Pendubot system subjects to both matched and unmatched uncertainty. An orthogonal decomposition method is adopted to deal with the system uncertainty. After decomposition, the mismatched part of the uncertainty “disappears”. For the matched part,

an adaptive law with a leakage term is adopted to estimate its upper bound. Based on that, an adaptive robust control law is developed. Through rigorous mathematical derivation, we show that the closed-loop system is uniformly bounded and uniformly ultimately bounded, without approximating or linearizing the original nonlinear dynamics. Simulation results suggest that the constraint can be effectively followed.

Author contributions. Cui Wei wrote the article. Ye-Hwa Chen, Tianyou Chai, and Jun Fu provided advice and supervision.

Financial support. This work was supported in part by National Natural Science Foundation of China under grants 62203215, 61991404, 61991400, and 61991402, National Key R&D Program of China under grant 2022YFB3305002, and the 2020 Science and Technology Major Project of Liaoning Province under grant 2020JH1/10100008.

Conflicts of interest. The authors declare no conflicts of interest exist.

Ethical considerations. No ethical issue with this paper.

References

- [1] M. Aminsafaei and M. H. Shafiei, "A robust approach to stabilization of 2-dof underactuated mechanical systems," *Robotica* **38**(12), 2221–2238 (2020).
- [2] S. H. Zabihifar, H. Navvabi and A. S. Yushchenko, "Dual adaptive neural network controller for underactuated systems," *Robotica* **39**(7), 1281–1298 (2021).
- [3] G. He, C. Zhang, W. Sun and Z. Geng, "Stabilizing the second-order nonholonomic systems with chained form by finite-time stabilizing controllers," *Robotica* **34**(10), 2344–2367 (2016).
- [4] H. Chen and N. Sun, "An output feedback approach for regulation of 5-dof offshore cranes with ship yaw and roll perturbations," *IEEE Trans. Ind. Electron.* **69**(2), 1705–1716 (2022).
- [5] H. Yin, Y. H. Chen and D. Yu, "Controlling an underactuated two-wheeled mobile robot: A constraint-following approach," *J. Dyn. Syst. Meas. Contr.* **141**(7), 071002–1–9 (2019).
- [6] R. Hota and C. Kumar, "Effect of design parameters on strong and immobilizing grasps with an underactuated robotic hand," *Robotica* **40**(11), 3769–3785 (2022). doi: [10.1017/S0263574722000601](https://doi.org/10.1017/S0263574722000601).
- [7] W. Xie, D. Cabecinhas, R. Cunha and C. Silvestre, "Robust motion control of an underactuated hovercraft," *IEEE Trans. Control Syst. Technol.* **27**(5), 2195–2208 (2018).
- [8] J. Zhang and G. Yang, "Fault-tolerant fixed-time trajectory tracking control of autonomous surface vessels with specified accuracy," *IEEE Trans. Ind. Electron.* **67**(6), 4889–4899 (2020).
- [9] J. Zhang and T. Chai, "Singularity-free continuous adaptive control of uncertain underactuated surface vessels with prescribed performance," *IEEE Trans. Syst. Man Cybern.: Syst.* **52**(9), 5646–5655 (2022). doi: [10.1109/TSMC.2021.3129798](https://doi.org/10.1109/TSMC.2021.3129798).
- [10] T. Chen, J. Shan and H. Wen, "Distributed adaptive attitude control for networked underactuated flexible spacecraft," *IEEE Trans. Aerosp. Electron. Syst.* **55**(1), 215–225 (2019).
- [11] M. W. Spong and D. J. Block, "The Pendubot: A mechatronic system for control research and education. In: *Proceedings of 1995 34th IEEE Conference on Decision and Control* (1995) pp. 555–556.
- [12] I. Fantoni, R. Lozano and M. W. Spong, "Energy based control of the Pendubot," *IEEE Trans. Autom. Contr.* **45**(4), 725–729 (2000).
- [13] T. Albahkali, R. Mukherjee and T. Das, "Swing-up control of the Pendubot: An impulse-momentum approach," *IEEE Trans. Robot.* **25**(4), 975–982 (2009).
- [14] D. Xia, L. Wang and T. Chai, "Neural-network-friction compensation-based energy swing-up control of Pendubot," *IEEE Trans. Ind. Electron.* **61**(3), 1411–1423 (2014).
- [15] D. Xia, T. Chai and L. Wang, "Fuzzy neural-network friction compensation-based singularity avoidance energy swing-up to nonequilibrium unstable position control of Pendubot," *IEEE Trans. Control Syst. Technol.* **22**(2), 690–705 (2014).
- [16] M. Eom and D. Chwa, "Robust swing-up and balancing control using a nonlinear disturbance observer for the Pendubot system with dynamic friction," *IEEE Trans. Robot.* **31**(2), 331–343 (2015).
- [17] C. Wei, T. Chai, X. Xin, X. Chen and Y. H. Chen, "A signal compensation-based robust swing-up and balance control method for the Pendubot," *IEEE Trans. Ind. Electron.* **69**(3), 3007–3016 (2022).
- [18] H. Yin, Y. H. Chen, J. Huang and H. Lü, "Tackling mismatched uncertainty in robust constraint-following control of underactuated systems," *Inf. Sci.* **520**, 337–352 (2020).
- [19] C. Wei, T. Chai, J. Yao and L. Wang, "Compensation signal driven adaptive balance control of the Pendubot," *Acta Autom. Sin.* **45**(6), 1146–1156 (2019).
- [20] R. Yu, Y. H. Chen, H. Zhao and H. Sun, "Uniform ultimate boundedness for underactuated mechanical systems as mismatched uncertainty disappeared," *Nonlinear Dyn.* **95**(4), 2765–2782 (2019).

- [21] Y. H. Chen, "On the deterministic performance of uncertain dynamical systems," *Int. J. Control* **43**(5), 1557–1579 (1986).
- [22] M. Corless and G. Leitmann, "Continuous state feedback guaranteeing uniform ultimate boundedness for uncertain dynamic systems," *IEEE Trans. Autom. Control* **26**(5), 1139–1144 (1981).